Catalysis Communications 172 (2022) 106537

Contents lists available at ScienceDirect

Catalysis Communications

journal homepage: www.elsevier.com/locate/catcom

Enzyme-inspired dry-powder polymeric catalyst for green and fast pharmaceutical manufacturing processes

Raquel Viveiros [a,b], Luísa B. Maia [a], Marta C. Corvo [c], Vasco D.B. Bonifácio [d], William Heggie [b], Teresa Casimiro [a,*]

[a] LAQV-REQUIMTE, Chemistry Department, NOVA School of Science & Technology, NOVA University of Lisbon, Campus de Caparica, 2829-516 Caparica, Portugal
[b] HOVIONE FarmaCiência SA, R&D, Sete Casas, 2674-506 Loures, Portugal
[c] I3N-CENIMAT, Material Science Department, NOVA School of Science & Technology, NOVA University of Lisbon, Campus de Caparica, 2829-516 Caparica, Portugal
[d] iBB-Institute for Bioengineering and Biosciences, Instituto Superior Técnico, Av. Rovisco Pais, 1, 1049-001 Lisboa, Portugal

ARTICLE INFO

Keywords:
Catalysis
Molecular recognition
Molecularly imprinted polymers
Artificial enzymes
Green chemistry
TEMPO

ABSTRACT

Catalysis in pharma manufacturing processes is typically homogeneous, expensive and with hard catalyst recovery/regeneration. Herein an enzyme-inspired dry-powder molecularly imprinted polymeric (MIP) system was designed for fast, selective oxidation of a cholesterol derivative and easy catalyst regeneration. The strategy involved the synthesis of a template-monomer (T:M) complex followed by the crosslinked polymerization in supercritical carbon dioxide ($scCO_2$). A 2,2,6,6-tetramethyl-1-piperidinyloxy (TEMPO)-MIP catalyst is obtained after the template cleavage from the matrix, and the oxidation of the N—H groups turns available TEMPO moieties within the MIP. The oxidation of benzyl alcohol, 5α-cholestan-3β-ol and cholic acid was fast, in high yield and with selective oxidation capacity.

1. Introduction

Enzymes are ubiquitous in nature and catalyze chemical reactions with a remarkable selectivity [1]. However, these high-cost enzymes are typically sensitive depending on their environment and can denature under harsh conditions. The preparation of engineered enzyme-like polymeric powder particles, with the same selectivity and catalytic performance of natural enzymes has been a major driving force in the development of synthetic counterparts that are able to work under extreme conditions without degradation. To achieve this goal, noble metals, cyclodextrins, affinity polymers and biomolecules (e.g. nucleic acids, antibodies and proteins) have been proposed to replace natural enzymes [2].

Affinity particles based on molecularly imprinted polymers (MIPs) have been investigated as artificial enzymes [3], thus providing high stability, long-lasting, reusable and low-cost alternatives for a wide range of applications. By taking advantage of the molecular imprinting technique (MIT), in which an affinity cavity is produced within a rigid crosslinked material, the cavity size, shape and functionality can be well defined by selecting the functional monomer and target template molecules. The template choice is key for a successful recognition and is of utmost importance, playing a crucial role in the materials performance.

Common approaches to MIP design are based in non-covalent, semi-covalent and covalent strategies [4,5], mainly differing in the established template-monomer interactions. Non-covalent imprinting is by far the easiest way to prepare MIPs, where only a template and functional and cross-linking monomers are required. In contrast, covalent imprinting is a much more challenging strategy since it requires a template-monomer complex (T-M), which is not always commercially available, such as bisphenol dimethacrylate (BPADM) [4]. T-M complexes need to be specifically designed and synthesized for a target molecule. In many cases, special storage and handling of these monomers is required due to inherent lack of stability. Consequently, the design and synthesis of covalently imprinted polymers for catalytic

Abbreviations: APIs, Active Pharmaceutical Ingredients; TEMPO, (2,2,6,6-Tetramethylpiperidin-1-yl)oxyl; $scCO_2$, supercritical carbon dioxide; MIPs, Molecularly Imprinted Polymers; T-M, template-monomer complex; BPADM, bisphenol dimethacrylate; TSAs, Transition State Analogues; GC-FID, Gas Chromatography With Flame Ionization Detection; TLC, thin layer chromatography; SEM, Scanning electron microscopy; FTIR, Fourier Transform Infrared Spectroscopy; FTIR-ATR, Fourier Transform Infrared Spectroscopy with Attenuated Total Reflectance; EPR, Electron Paramagnetic Resonance; GC–MS, Gas Chromatography Mass Spectrometry; CP/MAS – NMR, Cross-Polarization Magic Angle Spinning Carbon-13 Nuclear Magnetic Resonance..

* Corresponding author.
E-mail address: teresa.casimiro@fct.unl.pt (T. Casimiro).

https://doi.org/10.1016/j.catcom.2022.106537
Received 19 August 2022; Received in revised form 5 October 2022; Accepted 17 October 2022
Available online 18 October 2022

applications is more difficult but allows to produce more efficient and selective materials.

Enzyme mimics [6] have been achieved by taking advantage of affinity polymers produced using different approaches, namely non-covalent imprinting of i) transition state analogues (TSAs) [7], ii) enzymatic reaction products, iii) substrate analogues and iv) cofactors [8]. The TSA approach has drawbacks since it needs to be specific for a particular catalytic reaction. However, often TSAs cannot be used as templates due to high instability and a dummy TSA is generally used [9]. The molecular imprinting of enzymatic reaction products has shown notable results, with MIPs exhibiting the highest catalytic activity ever reported. Nitroxide-based MIPs using modified templates have been also explored [10], although without reaching the desired selectivity.

MIP-based catalysts have been produced as polymers or grafted on to a variety of supports by surface-imprinting techniques. However, all published works use a non-covalent imprinting approach and are focused on photocatalytic degradation applications. For example, surface imprinted layers on titanium particles were reported [11] to work as a photocatalyst for degradation of contaminants in aqueous solutions. This system comprises a covalent pre-functionalization of the support with silane coupling agents and further MIP layer grafting using organic solvents. Imprinted mesoporous silica-based catalysts, produced by a sol-gel method, have been used for cellulose hydrolysis c and to convert cellobiose into glucose [12]. Other examples include environment-friendly and low-cost imprinted magnetic nano-catalyst for degradation of polluting dyes [13] and MIP-layered TiO_2-functionalized particles, produced by a hydrothermal method, which improve the catalytic degradation of non-functionalized TiO_2 particles by 30% [14]. Other strategies have been proposed, with the aim of creating catalytic scaffolds, but involving non-selective catalytic processes, such as radical species immobilized on non-specific polymers [15], silica [16], carbon nanotubes [17], ionic liquids [18], deep eutectic solvents [19] or magnetic particles [20].

Homogeneous catalysts are widely used in industry, however the difficulties in the catalyst separation step from the final material, limit their application in an economic and environmental way. It is crucial to remove until trace levels of catalyst from the end product since their contamination is highly regulated, especially by the pharmaceutical industry. Even with the extensive use of techniques such as chromatography, distillation or extraction, the removal of trace amounts of catalyst remains a challenge. To overcome the separation drawbacks, researchers have investigated a wide range of strategies to produce heterogeneous catalyst systems, providing excellent stability (chemical and thermal), good accessibility, porosity, and the organic groups can be covalently anchored to the surface to provide catalytic centers, producing a robust material enough to withstand the harsh conditions and the catalyst can be reused several times [21].

Industry is seeking new, highly selective heterogeneous catalysts, environmentally friendly, reusable, longer lasting and affordable catalytic processes to replace current, less attractive homogeneous catalyst solutions. Allying molecular imprinting to catalytic processes can potentially meet this need, thus allowing the production of tailor-made, selective and cost-effective catalysts. $ScCO_2$ is a green alternative solvent that has been used in polymer synthesis and processing wherein many beneficial aspects are brought about in comparison to traditional approaches, being considered a green technology. This applies to the development of MIPs, where nano- to micron-sized homogeneous particles with highly controlled morphology and porosity, are obtained ready-to-use, in a single-step, as dry-powders in high purity without solvent residues [22–24].

Herein, green enzyme-inspired polymeric dry powder particles, were developed to work as catalysts in the oxidation of a cholesterol derivative. The followed synthetic route involved four steps: 1) the synthesis of a template:monomer (T:M) (2,2,6,6-tetramethylpiperidin-4-ol-cholesterol) complex; 2) the production of a cholesterol-imprinted polymer from T:M complex in supercritical carbon dioxide ($scCO_2$); 3) the cleavage the cholesterol from the matrix in $scCO_2$ and, 4) the polymer was then oxidized by 3-choroperbenzoic acid, to obtain the catalytic ability of the polymer. The final material has a dual-function MIP, combining affinity and catalytic ability: an empty cavity with size and shape complementary to cholesterol, produced by the cholesterol-MIP and; in the last step of their production (Fig. 1, compound 10) when the polymer was oxidized in N—H group, making to appear a 2,2,6,6-tetramethyl-1-piperidinyloxy (TEMPO) moiety entrapped into MIP matrix, providing a TEMPO-MIP catalyst.

TEMPO has several industrial applications as selective oxidation catalyst for the production of pharmaceuticals, flavors, fragrances and agrochemicals [25]. Specially, TEMPO is used for oxidations of alcohols to aldehydes, ketones or carboxylic acids [26]. Cholesterol was used as a cheap starting molecule to produce, in the end, a large affinity cavity within the TEMPO-MIP, providing a cavity size large enough to promote the diffusion and the oxidation of the selected alcohol-based molecules, from small (benzyl alcohol) to larger molecules (5α-cholestan-3-β-ol), envisaging their potential use in other alcohol-based oxidations.

2. Experimental section

2.1. Materials

Available at Supporting Information.

2.2. Synthesis

The synthesis and characterization of intermediate monomers **3–7**, polymer precursors **8** and **9** and the final TEMPO-MIP **10** is described below. FTIR and NMR spectra can be found at Supporting Information (Fig. S1-S10).

2.2.1. Compound 3

The epoxide intermediate (**3**) [27] was obtained as follow. KOH (9.1 g, 16.2 mmol) dissolved in 6.35 mL of water, toluene (16 mL), **2** (5.0 g, 31.9 mmol) and TBABr (1.2 g, 3.7 mmol) are mixed in a bottom-rounded flask and the mixture heated to 55 °C. Epichlorohydrin (5 mL, 63.8 mmol) is then added dropwise, and the mixture stirred vigorously keeping the temperature constant at 55 °C for 10 h. The reaction was followed by TLC, using a mixture of ethyl acetate/methanol (50:50) as the eluent phase. Next, ice was added to the reaction mixture while the mixture was immersed in an ice bath. The phases were separated, and the aqueous phase was further extracted with ethyl acetate (10 × 10 mL). The combined organic phases were dried over anhydrous Na_2SO_4, filtered and the solvent evaporated. A yellow oil was obtained in 61% yield. IR (film) ν_{max} (cm^{-1}): 3500 (OH, NH), 3000 (CH), 2999 (CH) 2888 (CH), 1500, 1400, 1250, 1100 (CH-O), 800. ^{1}H NMR ($CDCl_3$, 400 MHz): 4.01–3.96 (1H, m, H_a), 3.74–3.69 (1H, m, $H_{d/d'}$), 3.44.3.40 (1H, m, $H_{d/d'}$), 3.1 (1H, bs, H_e), 2.76 (1H, t, $J = 4.0$ Hz, $H_{f/f'}$), 2.57 (1H, t, $J = 4.0$ Hz, $H_{f/f'}$), 1.95–1.86 (2H, m, $H_{b/b'}$), 1.14 (6H, s, H_c), 1.11 (6H, s, H_c), 1.14 (6H, s, H_c), 0.98 (2H, t, $J = 8.0$ Hz, $H_{b/b'}$).

2.2.2. Compound 5

Cholesteryl hydrogen succinate (**5**) was synthesized following a reported protocol [28]. Cholesterol (**4**) (2 g, 5.2 mmol) and succinic anhydride (0.6 g, 6.3 mmol) were dissolved in 25 mL of 1,4-dioxane. Then, DMAP (0.7 g, 6.3 mmol) was added, and the reactional mixture was stirred at room temperature for 24 h. At the end of reaction, a solution of 6 M HCl was added dropwise to precipitate the product. A white fluffy solid was obtained in 90.5%. ^{1}H NMR ($CDCl_3$, 400 MHz): 5.37 (1H, bs, H_a), 4.63 (1H, bs, H_b), 2.64 (2H, dd, $J = 4.0$, 10.0 Hz, $H_{d/d'}$), 2.02–0.85 (42H, m, $H_{cholesterol}$), 0.67 (3H, s, H_c).

2.2.3. Compound 6

Compound **6** was synthesized in one step from cholesteryl succinate (**5**) following a reported protocol [29]. Briefly, cholesteryl succinate (**5**)

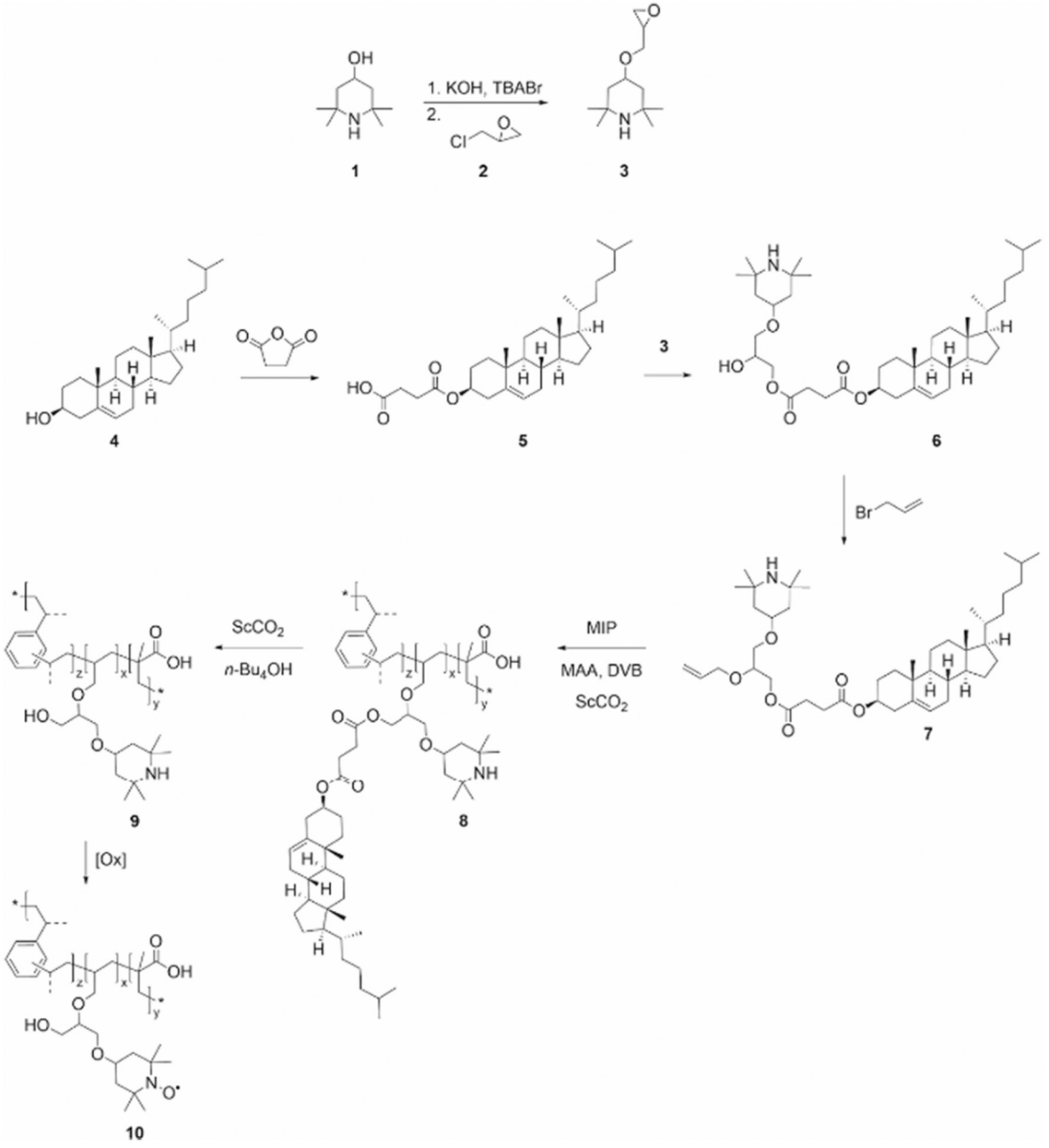

Fig. 1. Schematic synthesis of enzyme-inspired polymer particles, TEMPO-MIP **10**.

(3.4 g, 6.7 mmol) and epoxide **3** (1.26 g, 5.89 mmol) were added to [bmim]Br (3.1 g, 14.2 mmol). The resulting mixture was heated in an oil bath at 75 °C and stirred for 12 h. At the end of reaction, the mixture was cooled to room temperature. Next, brine was added to the reaction mixture and kept under stirring for 10 min. Finally, the product was extracted with chloroform, the organic phase was dried over anhydrous Na_2SO_4, filtered and the solvent evaporated. A white sticky solid was obtained in 95.8%. IR (film) ν_{max} (cm^{-1}): 3416 (OH, NH), 2942 (CH), 1728 (O-C=O), 1463, 1384, 1171, 800. ^{1}H NMR (400 MHz, $CDCl_3$) δ (ppm): 5.35 (bs, 1H), 4.20–4.00 (m, 1H), 3.98–3.93 (m, 1H), 3.74–3.46 (m, 5H), 2.63–2.52 (m, 2H), 2.31–2.28 (m, 2H) 2.02–0.85 (m, 54H), 0.67 (s, 3H). ^{13}C NMR (100.9 MHz, CDCl3) δ (ppm): 172.93, 172.40, 171.70, 140.77, 139.82, 139.48, 122.75, 122.65, 122.42, 121.66, 74.48, 74.27, 73.71, 71.54, 71.74, 70.33, 69.49, 68.85, 65.77, 56.75, 56.66, 56.14, 50.12, 49.99, 42.28, 39.77, 39.70, 39.49, 37.24, 36.93, 36.58, 36.55, 36.48, 36.17, 35.76, 31.88, 31.83, 31.64, 28.20, 27.98, 27.72, 24.27, 23.80, 22.79, 22.53, 21.06, 21.00, 19.37, 19.28, 18.69, 11.83.

2.2.4. Compound 7

Compound **7** was synthesized by allylation of compound **6** following a reported protocol [30]. In brief, NaH (185 mg, 4.62 mmol) was added to compound **6** (1.65 g, 2.31 mmol) in 50 mL of anhydrous THF, under argon atmosphere, and the mixture stirred at room temperature for 5 min. The reaction mixture was further stirred for more 30 min at room temperature. Next, allyl bromide (400 μL, 4.62 mmol) was added to the reaction mixture and stirred at room temperature for 42 h. After this period, ice was added to the reaction and the mixture evaporated. The mixture was then re-suspended in methanol and insoluble materials were removed by filtration and the organic phase evaporated. A light-yellow sticky solid was obtained in 61% yield. IR (film) ν_{max} (cm^{-1}): 3500 (OH, NH), 3000 (CH), 2990 (CH), 1700 (COO), 1400 (CH-O) 1300, 1000 (CH-O), 800 (CH-O). NMR (400 MHz, DMSO-d_6) δ (ppm): 6.46 (m, 1H), 6.05 (m, 1H), 5.26–5.01 (m, 2H), 4.61 (m, 1H), 4.20–4.00 (m, 1H), 3.98–3.93 (m, 1H), 3.97 (m, 2H), 3.74–3.46 (m, 5H), 2.63–2.52 (m, 2H), 2.31–2.28 (m, 2H), 2.02–0.85 (m, 54H), 0.67 (s, 3H).

2.2.5. Synthesis of precursor affinity polymer particles 8

The precursor (cholesterol-templated) affinity polymer particles were obtained by a $scCO_2$-assisted polymerization. Methacrylic acid (MAA) was used as co-monomer and divinylbenzene (DVB) as crosslinker and the reaction was performed using a molar composition of 1:4:20 respectively to template-monomer (T:M) complex:co-monomer: crosslinker in which 150.3 mg of **7** were dissolved in 1.5 mL of DMF, 67.6 μL of MAA and 567 μL of DVB and AIBN (1 wt% of total monomers) were introduced in a 33 mL high-pressure cell and CO_2 was added under stirring for 24 h at 65 °C and 28 MPa. A single phase was observed. After polymerization, a homogeneous fluffy white powder was obtained in 26.5% yield.

2.2.6. Synthesis of affinity polymer particles 9

The removal of cholesterol from **8** was also performed using a $scCO_2$-assisted methodology. In a typical experiment, 369 mg of MIP (**8**), *n*-Bu_4NOH 1.0 M in methanol (202.5 μL, 1.6 mmol) and a magnetic stir bar were introduced into a 33 mL high-pressure cell. The cell was immersed in a thermostated water bath at 65 °C and pressurized with CO_2 until a final pressure of 20 MPa was reached. After 24 h of reaction the polymer was washed with a fresh stream of CO_2 for 1 h.

2.2.7. Production of TEMPO-MIP 10

In a typical procedure, 49.6 mg of the oxidizing agent, 3-choroperbenzoic acid (*m*-CPBA) was added to 105.1 mg of precursor **9**. After the addition of the oxidant, the polymer did not exhibit any differences in color and appearance. EPR analysis was performed to confirm the formation of TEMPO radicals (Fig. 3).

2.3. Catalytic assays

2.3.1. Benzaldehyde oxidation

Benzyl alcohol (6.74 μM) in dichloromethane (20 mL), KBr (0.5 M) in water (5 mL), 4-methoxyacetophenone (500 mg, internal standard) and **10** (74.9 mg, placed inside a dialysis membrane) were added to a round-bottom flask. The reaction mixture was stirred (300 rpm) at 0 °C before the addition of aqueous NaOCl (0.35 M, pH 8.7, 90 mL). Sample aliquots were regularly taken from the organic phase for a 20-min period. The reaction was followed by TLC, and the plates sprayed with 2,4-DNP solution to detect the formation of benzaldehyde.

2.3.2. 5α-Cholestan-3-β-ol oxidation

5α-cholestan-3-β-ol (6.74 μM) in dichloromethane (20 mL), KBr (0.5 M) in water (5 mL), *n*-dodecane (500 mg, internal standard) and **10** (74.9 mg, packed inside a SnakeSkin™ dialysis membrane) were added to a round-bottom flask. The reaction mixture was stirred (300 rpm) at 0 °C before adding aqueous NaOCl (0.35 M, pH 8.7, 90 mL). Sample aliquots were regularly taken for 15 min and followed by TLC, and the plates sprayed with a 2,4-DNP solution to detect the formation of cholestanone. In a second test, a 10× concentration of 5α-cholestan-3-β-ol (67.4 μM) was used. The samples were further analyzed after derivatization, following a reported protocol (Fig. S11, SI) [31] using cholestane as an internal standard.

2.3.3. Cholic acid oxidation

Cholic acid (6.74 μM) in chloroform (20 mL), KBr (0.5 M) in water (5 mL) and 74.9 mg of **10** (packed inside a SnakeSkin™ dialysis membrane) were added to a round-bottom flask. The reaction mixture was stirred (300 rpm) at 0 °C before addition of aqueous NaOCl (0.35 M, pH 8.7, 90 mL). Sample aliquots were regularly taken for 30 min and followed by TLC, and the plates sprayed with 2,4-DNP solution to detect product formation. The samples were further derivatized, following a reported protocol [32] (Fig. S12, SI) using hyodeoxycholic acid as an internal standard. The quantification of the oxidation products was further accessed by GC-FID analysis using a Konik, HRGC 4000 B instrument.

2.3.4. Turnover number (TON) and turnover frequency (TOF) calculations [33]

Considering that TEMPO has one catalytic active site, the TON and TOF are calculated related to their moles as follows:

$$TON = \frac{n_{\text{alcohol}} \cdot \eta}{n_{TEMPO}}$$

where the n_{alcohol} are the number of moles of alcohol, η, the yield of the reaction and n_{TEMPO} the number of moles of TEMPO.

$$TOF\ (h^{-1}) = \frac{TON}{Time\ of\ reaction\ (h)}$$

2.4. Methods

Available at Supporting Information.

3. Results and disscussion

3.1. Production of enzyme-inspired polymer particles

As a strategy to develop new and green enzyme-inspired polymeric powder particles, a 4-hydroxy-TEMPO moiety was immobilized in a predesigned MIP pocket to function as a selective oxidation catalyst. The synthetic route involved the preparation of a TEMPO-templated monomer **7**, which upon a $scCO_2$-assisted polymerization and template removal ultimately led to the desired catalyst, TEMPO-MIP **10** (Fig. 1).

The synthesis started with the preparation of key intermediates **3** and **5**. The reaction of **3** with **5** followed a green ionic liquid-catalyzed epoxide ring opening methodology [29], which furnished **6** in excellent yield. Allylation of **6** led to monomer **7**, which was readily copolymerized with MAA, using DVB as a crosslinker and AIBN as an initiator, in $scCO_2$. This polymerization led to a precursor copolymer **8** carrying the cholesterol template and displaying a physical appearance consistent with reported polymers obtained by $scCO_2$-assisted polymerization [22]. Although cloud points or phase diagrams studies were not investigated, a very important aspect in this polymerization is the solubility of the T-M complex in porogenic $scCO_2$. The solvent plays an important role in the formation of porous structures within the affinity polymer particles and will determine the morphological properties such as porosity and surface area [34]. To proceed, template removal was needed. The cleavage of cholesterol from **8** was also performed in $scCO_2$. For the first time, we describe the hydrolysis of cholesterol from a semi-covalent MIP crosslinked in $scCO_2$, taking advantage of the solubility of cholesterol in $scCO_2$ and using methanol as co-solvent. Following our protocol, using *n*-Bu_4NOH 1 M in methanol, polymer **9** was successfully obtained [35]. The *n*-Bu_4NOH–methanol–$scCO_2$ system is a very effective hydrolysis method for highly crosslinked polymers due to a synergic effect: (i) *n*-Bu_4NOH is the hydroxide source, (ii) CO_2 diffusivity power increases the hydrolysis efficiency, and (iii) methanol with high solvent power for cholesterol enhances its desorption from highly crosslinked matrices. After hydrolysis, the cholesterol removal efficiency (~ 90%) was determined by HPLC [36], thus showing that the $scCO_2$-assisted cholesterol cleavage is a highly efficient process.

Fig. 2 shows a scanning electron microscopy (SEM) image of the affinity polymer particles **9**. As it can be seen, the particles were obtained as small agglomerates of primary nanoparticles, which is typically observed in precipitation polymerization in $scCO_2$ [22,23].

The FTIR spectrum of **9** (Fig. S9, SI) shows a new broad band at 3345 cm^{-1}, characteristic of hydroxyls groups, which confirms a successful hydrolysis. High-resolution solid-state NMR (^{13}C-CP/MAS) [37] was also performed to further characterize polymers **8** and **9**, and in particular to evaluate the cleavage of the cholesterol from the matrix (Fig. S10, SI).

A comparative CP/MAS-NMR analysis of cholesterol and polymers **8** and **9** was performed. The broadness of the spectra is typical of an

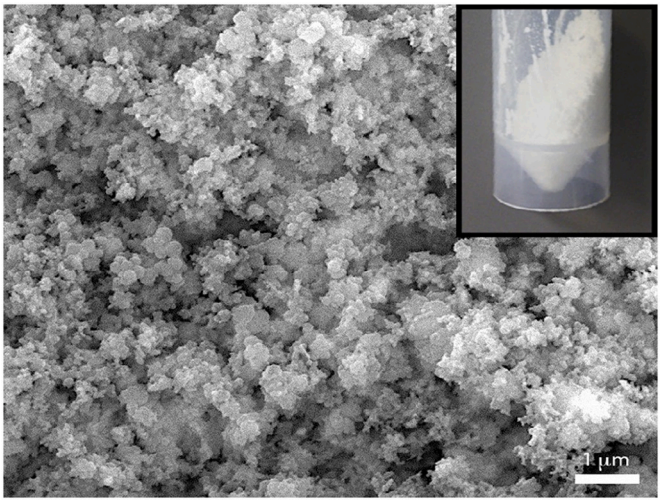

Fig. 2. SEM image of TEMPO-MIP particles. The inset shows a picture of the polymer collected at the end of the polymerization.

amorphous polymer. Polymer **8** displays peaks at 185.6, 183 and 172 ppm (esters carbonyls), at 122, 123, 128 and 142 ppm (aromatic carbons, DVB crosslinker), and in the region 10–15 ppm (methyl groups, MAA). The cholesterol within the matrix shows peaks in the region 15–60 ppm, at 121 ppm and 140.8 ppm). There are three peaks around 200 ppm, marked with (*), which are spinning side bands (ssb). The peaks at 180 ppm and 175 ppm probably correspond to a small molecule, perhaps bicarbonate entrapped in the matrix generated by the reaction of $scCO_2$ and *n*-Bu_4NOH. The removal of cholesterol from **8** was found to be very efficient since the characteristic ester peaks in the region 172–186 ppm are absent, in accordance with the proposed structure of **9**, as well as the peaks from cholesterol (more easily observable in the region around 15 ppm).

Additionally, nitrogen porosimetry was also assessed (isotherm and BET parameters, Fig. S13, SI). Although the BET surface area is consistent with previous work [22], pore volume and average pore diameter were significantly higher than the values typically obtained for MIPs prepared in $scCO_2$. Nevertheless, the contribution from cholesterol, a larger template, should not be ruled out.

Finally, enzyme-inspired polymeric powder particles, TEMPO-MIP **10**, were synthesized by simple oxidation of **9**. This reaction is well described in literature using 3-choroperbenzoic acid (*m*-CPBA) as the oxidant [38]. To quantify the TEMPO radical species in **10**, an EPR analysis was also performed (Fig. 3).

The EPR spectrum is characteristic of a nitrogen-centered radical (I(N) = 1, $g_{av} \approx 2$) present in a rigid matrix ($g_1 \neq g_2 \neq g_3$; anisotropic signal), like other TEMPO-containing systems (Table 1). The absence of clear nitrogen-nitrogen super-hyperfine interactions suggests that each radical center is more than ≈15 Å apart. The concentration of TEMPO radicals in **10** was estimated to be 32.9 μmol.g^{-1}.

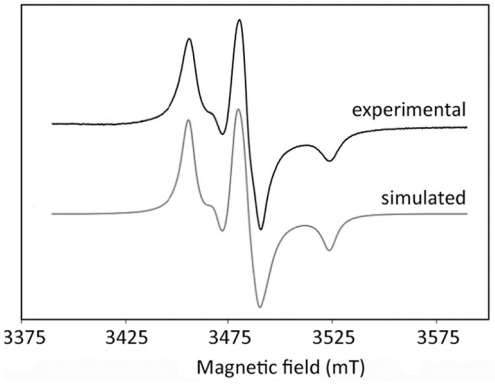

Fig. 3. Experimental EPR spectrum of TEMPO-MIP **10** and its simulation using the parameters summarized in Table 1.

3.2. Catalyst performance

3.2.1. Conversion of benzyl alcohol into benzaldehyde

Firstly, to evaluate the catalytic activity of **10**, a preliminary assay using benzyl alcohol as a model substrate, small enough to fit into the imprinted cholesterol pocket. A hypochlorite solution was used to regenerate the NO radicals [40]. The catalytic performance of **10** in oxidation reactions was evaluated by GC analysis (Fig. 4). The reaction was found to occur in quantitative yield and much faster (ca. 8 min), in comparison with the same reaction performed using other non-molecularly imprinted TEMPO-based catalysts [40–42]. A turnover number (TON) of 5.47 and a turnover frequency (TOF) of 41.03 h^{-1} were achieved, better than other reported TEMPO polymeric catalysts [43–45]. No oxidation was observed in a control experiment without **10**.

The several catalytic systems previously developed using TEMPO as the oxidant species, all anchor the TEMPO on the surface, and none are designed to be specific. Also, most of them have low stability, thus precluding recycling over long periods of time. In the present strategy we have incorporated the TEMPO units tethered in well-defined pockets of a crosslinked polymer, providing a very stable and reusable matrix.

3.2.2. Conversion of 5α-cholestan-3-β-ol into 5α-cholestan-3-one

After establishing the oxidation protocol using **10** and benzaldehyde, the selective oxidation of target cholesterol derivatives was investigated. Therefore, recycled **10** was used as catalyst for the oxidation of 5α-cholestan-3-β-ol to 5α-cholestan-3-one (Fig. 5).

Two different concentrations were evaluated, and once again an outstanding catalytic performance was observed. After only 15 min of reaction time ~ 70% of 5α-cholestan-3-one was obtained. However, when the concentration of 5α-cholestan-β-ol was increased ten times a poor yield was obtained (~12%). For the lower concentration, a turnover number (TON) of 2.68 and a turnover frequency (TOF) of 10.72 h^{-1} were achieved better than other reported TEMPO polymeric catalysts [43–45].This is not surprising as the rate of the reaction is only proportional to the concentration of the active sites, thus limiting substrate concentration. Concentrations above this maximum value will not influence this absolute achievable rate. Even so, the catalyst to substrate ratio using a higher 5α-cholestan-3-β-ol concentration compares favorably with other reported methods [46,47]. For the quantities indicated, good conversion yield would take around 2 h.

3.2.3. TEMPO-MIPs selectivity – cholic acid

The selectivity of TEMPO-MIP **10** was also investigated using cholic

Table 1
EPR parameters of TEMPO radicals in TEMPO-MIP **10** and similar systems.

Samples	g-factor*1			Hyperfine Constant*2		
	g_1	g_2	g_3	a_1^N (mT)	a_2^N (mT)	a_3^N (mT)
TEMPO-MIP **10** (this work*3)	2.0105	2.0072	2.0038	0.80	0.80	3.38
TEMPO grafted on silica [38]	2.0084	2.0053	2.0019	0.71	0.71	3.71
TEMPO in a lipid phase [39]	2.0098	2.0068	2.0025	0.65	0.50	3.56

*1: g_1, g_2 and g_3 stand for the low-field, medium-field and high-field lines, respectively.
*2: Hyperfine constants arising from the coupling with nitrogen atom; a_1^N, a_2^N, and a_3^N stand for the splitting of low-field, medium-field and high-field lines, respectively.
*3: Simulation as described in section *2.4 Methods* (SI).

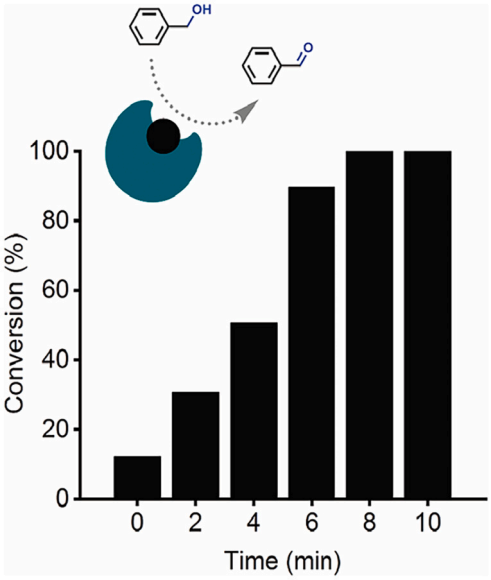

Fig. 4. Catalytic performance of TEMPO-MIP **10** in the oxidation of benzyl alcohol to benzaldehyde.

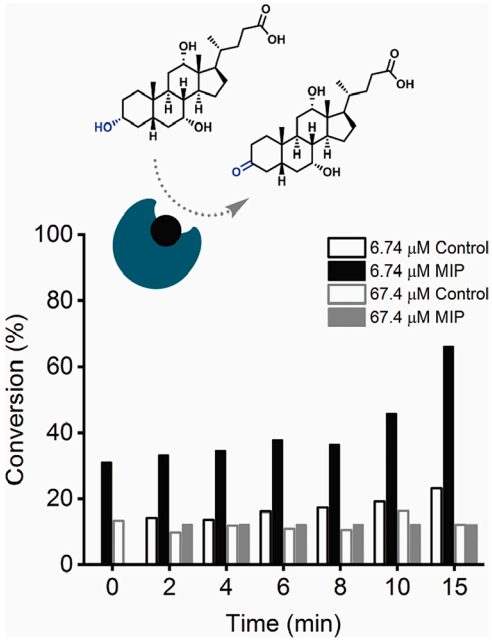

Fig. 5. Catalytic performance of enzyme-like polymer particles for the oxidation of 5α-cholestan-3-β-ol using different concentrations (6.74 μM and 67.4 μM).

acid. Cholic acid has three oxidizable hydroxyl groups in the cholesterol skeleton (Fig. 6). In addition, the A and B rings are fused in a cis fashion, which differs from trans cholesterol derivatives configurations. Thus, is not expected that cholic acid, having a higher 3D volume, would fit better in the MIP cavities than cholesterol.

Although TEMPO-MIP **10** can oxidize cholic acid to some extent, this oxidation was found to be unspecific since several oxidation products were detected (Fig. S14-S15, SI). The most intense peak observed appears at t_R = 19.26 min, which corresponds to dehydrocholic acid (Fig. S15-S16, SI). The corresponding fragmentation pattern is shown in Table 2.

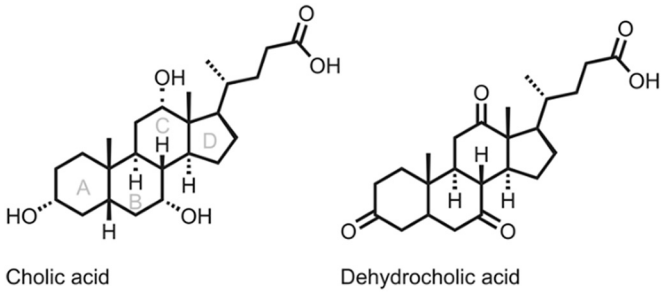

Fig. 6. Chemical structures of cholic and dehydrocholic acids.

Table 2
Fragmentation patterns of cholic acid (CA) and dehydrocholic acid (DHCA) determined as their trimethylsilyl(oxime)ether/ester derivatives by GC–MS.

Sample	M_w[a]	t_R (min)	Selective fragment ions (*m/z*)		
			$[M]^+$	$[M-15]^+$	Other abundant fragments
CA	408.58	4.64	696.5	681.6	$[M-2TMSOH]^+$ = 516.4 $[M-(2TMSOH + Si(CH3)4)]^+$ = 428.4 $[M-3TMSOH]^+$ = 426.4
DHCA	402.53	19.26	n.d.	n.d.	$[M-TMS]^+$ = 662.6 $[M-(TMS + CH3)]^+$ = 647.6

[a] Molecular weight (M_w) of the underivatized compound; t_R = retention time; $[M]^+$ = molecular ion; n.d. = not detected.

4. Conclusions

We can conclude that the minimal oxidation of the cholic acid hydroxyl groups by TEMPO-MIP **10** is indicative of a catalytic system highly specific for cholestanol derivatives in this molecular weight range. Such selectivity, combined with faster reaction times, makes enzyme-inspired polymeric powder particles (TEMPO-MIPs) a new generation of cheap greener heterogeneous catalysts with high potential for industrial applications.

Credit author statement

Raquel Viveiros: Methodology; Investigation; Writing- original draft.
Luísa Maia: Investigation.
Marta C. Corvo: Investigation.
Vasco D.B. Bonifácio: Investigation, Methodology; supervision.
William Heggie: Conceptualization; Methodology; supervision.
Teresa Casimiro: Conceptualization; Resources; Supervision; Writing, Reviewing and Editing.

Declaration of Competing Interest

The authors declare that they have no known competing financial interests or personal relationships that could have appeared to influence the work reported in this paper.

Data availability

No data was used for the research described in the article.

Acknowledgements

The authors thank financial support from Fundação para a Ciência e a Tecnologia, Ministério da Ciência, Tecnologia e Ensino Superior (FCT/MCTES Portugal), through project PTDC/EQU-EQU/32473/2017, a Principal Investigator contract IF/00915/2014 (T.C.), and a doctoral grant SFRH/BDE/51907/2012, a partnership from FCT/MCTES and the

pharmaceutical company HOVIONE (R.V.). L.B.M. would like to acknowledge for FCT/MCTES funding with reference CEECIND/03810/2017. The NMR spectrometers in LabNMR@Cenimat are part of the National NMR Facility, supported by FCT (ROTEIRO/0031/2013 - PINFRA/22161/2016), co-financed by FEDER through COMPETE 2020, POCI, and PORL and FCT through PIDDAC (POCI-01-0145-FEDER-007688; UID/CTM/50025/2020-2023). The Associate Laboratory Research Unit for Green Chemistry - Clean Technologies and Processes - LAQV is financed by national funds from FCT/MCTES (UIDB/QUI/50006/2020) and cofunded by the ERDF under the PT2020 Partnership Agreement (POCI-01-0145-FEDER-007265). We also acknowledge Dr. Luz Fernandes, REQUIMTE analytical services, for GC analysis.

Appendix A. Supplementary data

Supplementary data to this article can be found online at https://doi.org/10.1016/j.catcom.2022.106537.

References

[1] S.F. Sousa, A.R. Calixto, P. Ferreira, M.J. Ramos, C. Lim, P.A. Fernandes, Activation free energy, substrate binding free energy, and enzyme efficiency fall in a very narrow range of values for most enzymes, ACS Catal. 10 (2020) 8444–8453.
[2] D. Jiang, D. Ni, Z.T. Rosenkrans, P. Huang, X. Yan, W. Cai, Nanozyme: new horizons for responsive biomedical applications, Chem. Soc. Rev. 48 (2019) 3683–3704.
[3] L. Marchetti, M. Levine, Biomimetic catalysis, ACS Catal. 1 (2011) 1090–1118.
[4] T. Ikegami, T. Mukawa, H. Nariai, T. Takeuchi, Bisphenol A-recognition polymers prepared by covalent molecular imprinting, Anal. Chim. Acta 504 (2004) 131–135.
[5] Y. Han, J. Tao, N. Ali, A. Khan, S. Malik, H. Khan, C. Yu, Y. Yang, M. Bilal, A. A. Mohamed, Molecularly imprinted polymers as the epitome of excellence in multiple fields, Eur. Polym. J. 179 (2022), 111582.
[6] S. Liu, P. Du, H. Sun, H. Yu, Z. Wang, Bioinspired supramolecular catalysts from designed self-assembly of DNA or peptides, ACS Catal. 10 (2020) 14937–14958.
[7] C. Philip, K.S. Devaky, Multiwalled carbon nanotubes with surface grafted transition state analogue imprints as chymotrypsin mimics for the hydrolysis of amino acid esters: synthesis and kinetic studies, Mol. Catal. 436 (2017) 276–284.
[8] S. Muratsugu, S. Shirai, M. Tada, Recent progress in molecularly imprinted approach for catalysis, Tetrahedron Lett. 61 (151603) (2020) 1–16.
[9] O. Brüggemann, Chemical reaction engineering using molecularly imprinted polymeric catalysts, Anal. Chim. Acta 435 (2001) 197–207.
[10] K.-A. Hansen, J.P. Blinco, Nitroxide radical polymers – a versatile material class for high- tech applications, Polym. Chem. 9 (2018) 1479–1516.
[11] H. Xiaubin, Patent US2015174568 - Molecularly Imprinted Catalysts and Methods of Making and Using the same, 2015.
[12] S. Roth, D. Lee, Patent US2012136180 - Imprinted Biomimetic Catalysts for Cellulose Hydrolysis, 2012.
[13] Patent CN104128207 - Preparation Congo red pseudo template imprinted core-shell magnetic nano catalyst degradation, 2014.
[14] Patent CN103611520 - Method for Preparing Molecular Imprinting-Doped TiO_2 with High Catalytic Degradation Activity under Visible Light, 2014.
[15] H. Liang, M. Cao, D. Yang, T. Sun, X. Chu, S. Liu, Polyamidoamine immobilized TEMPO mediated oxidation of cellulose: effect of macromolecular catalyst structure on the reaction rate, oxidation degree and degradation degree, Fibers Polym. 21 (2020) 1251–1258.
[16] J.S. Schulze, J. Migenda, M. Becker, S.M.M. Schuler, R.C. Wende, P.R. Schreiner, B. M. Smarsly, TEMPO-functionalized mesoporous silica particles as heterogeneous oxidation catalysts in flow, J. Mater. Chem. A 8 (2020) 4107–4117.
[17] C. Gambarotti, H.R. Bjørsvik, Amino-TEMPO grafted on magnetic multi-walled nanotubes: an efficient and recyclable heterogeneous oxidation catalyst, Eur. J. Org. Chem. 6 (2019) 1405–1412.
[18] L. Wylie, Z.L. Seeger, N. Hancock, E.I. Izgorodina, Increased stability of nitroxide radicals in ionic liquids: more than a viscosity effect, Phys. Chem. Chem. Phys. 21 (2019) 2882–2888.
[19] G. Carmine, A.P. Abbott, Dá Carmine, Deep eutectic solvents: alternative reaction media for organic oxidation reactions, React. Chem. Eng. 6 (2021) 582–598.
[20] T. Sun, H. Liang, S. Liu, E. Tang, C. Fu, Magnetic nanoparticles modified by polyamidoamine-immobilized TEMPO for catalytic oxidation of monomethoxy poly (ethylene glycol), J. Nanopart. Res. 22 (2020) 1–11.
[21] V. Polshettiwar, R.S. Varma, Green chemistry by nano-catalysis, Green Chem. 12 (2010) 743–775.
[22] R. Viveiros, M.I. Lopes, W. Heggie, T. Casimiro, Green approach on the development of *lock-and-key* polymers for API purification, Chem. Eng. J. 308 (2017) 229–239.
[23] R. Viveiros, V.D.B. Bonifácio, W. Heggie, T. Casimiro, Green development of polymeric dummy artificial receptors with affinity for amide-based pharmaceutical impurities, ACS Sustain. Chem. Eng. 7 (2019) 15445–15451.
[24] R. Viveiros, K. Karim, S.A. Piletsky, W. Heggie, T. Casimiro, Development of a molecularly imprinted polymer for a pharmaceutical impurity in supercritical CO_2: rational design using computational approach, J. Clean. Prod. 168 (2017) 1025–1031.
[25] R. Ciriminna, M. Pagliaro, Industrial oxidations with organocatalyst TEMPO and its derivatives, Org. Process. Res. Dev. 14 (2010) 245–251.
[26] G. Szekely, M.C.A. De Sousa, M. Gil, F.C. Ferreira, W. Heggie, Genotoxic impurities in pharmaceutical manufacturing: sources, regulations, and mitigation, Chem. Rev. 115 (2015) 8182–8229.
[27] L.C. Dias, L.S. Farina, M.A.B. Ferreira, Stereoselective total synthesis of the potent anti-asthmatic compound CMI-977 (LDP-977), J. Braz. Chem. Soc. 24 (2013) 184–190.
[28] S.-W. Lee, M.-H. Seo, M.-H. Hyun, D.-H. Chang, J. Yu, J.-K. Kim, H.-J. Yoon, WO2005040247 - Polymeric Composition for Drug Delivery, 2005.
[29] M.N.S. Rad, S. Behrouz, The base-free chemoselective ring opening of epoxides with carboxylic acids using [bmim]Br: a rapid entry into 1,2-diol mono-esters synthesis, Mol. Divers. 17 (2013) 9–18.
[30] Y. Ahn, Y. Jang, N. Selvapalam, G. Yun, K. Kim, Supramolecular velcro for reversible underwater adhesion, Angew. Chem. Int. Ed. 52 (2013) 3140–3144.
[31] C. Guitart, J.W. Readman, Critical evaluation of the determination of pharmaceuticals, personal care products, phenolic endocrine disrupters and faecal steroids by GC/MS and PTV-GC/MS in environmental waters, Anal. Chim. Acta 658 (2010) 32–40.
[32] Á. Sebok, K. Sezer, A. Vasanits-Zsigrai, A. Helenkár, G. Záray, I. Molnár-Perl, Gas chromatography-mass spectrometry of the trimethylsilyl (oxime) ether/ester derivatives of cholic acids: their presence in the aquatic environment, J. Chromatogr. A 1211 (2008) 104–112.
[33] A. Elhage, A.E. Lanterna, J.C. Scaiano, Catalytic farming: reaction rotation extends catalyst performance, Chem. Sci. 10 (2019) 1419–1425.
[34] D. Refaat, M.G. Aggour, A.A. Farghali, R. Mahajan, J.G. Wiklander, I.A. Nicholls, S. A. Piletsky, Strategies for molecular imprinting and the evolution of MIP nanoparticles as plastic antibodies — synthesis and applications, Int. J. Mol. Sci. 20 (2019) 1–21.
[35] M. Soares da Silva, R. Viveiros, A. Aguiar-Ricardo, V.D.B. Bonifácio, T. Casimiro, Supercritical fluid technology as a new strategy for the development of semi-covalent molecularly imprinted materials, RSC Adv. 2 (2012) 5075–5079.
[36] L.C. Bauer, D.A. De Santana, M.S. Dos Macedo, A.G. Torres, N.E. De Souza, J. I. Simionato, Method validation for simultaneous determination of cholesterol and cholesterol oxides in milk by RP-HPLC-DAD, J. Braz. Chem. Soc. 25 (2014) 161–168.
[37] J. Brus, M. Urbanova, J. Czernek, M. Pavelkova, K. Kubova, J. Vyslouzil, S. Abbrent, R. Konefal, J. Horsky, D. Vetchy, J. Vyslouz, P. Kulich, Structure and dynamics of alginate gels cross-linked by polyvalent ions probed via solid state NMR spectroscopy, Biomacromolecules 18 (2017) 2478–2488.
[38] K. Nakahara, S. Iwasa, M. Satoh, Y. Morioka, J. Iriyama, M. Suguro, E. Hasegawa, Rechargeable batteries with organic radical cathodes, Chem. Phys. Lett. 359 (2002) 351–354.
[39] T. Wiegand, M. Sajid, G. Kehr, G. Erker, H. Eckert, Solid-state NMR strategies for the structural characterization of paramagnetic NO adducts of frustrated Lewis pairs (FLPs), Solid State Nucl. Magn. Reson. 61–62 (2014) 19–27.
[40] M. Gilhespy, M. Lok, X. Baucherel, Polymer-supported nitroxyl radical catalysts for the hypochlorite and aerobic oxidation of alcohols, Catal. Today 117 (2006) 114–119.
[41] A. Schatz, R.N. Grass, W.J. Stark, O. Reiser, TEMPO supported on magnetic C/Co-nanoparticles: a highly active and recyclable organocatalyst, Chem. - A Eur. J. 14 (2008) 8262–8266.
[42] B. Karimi, E. Badreh, SBA-15-functionalized TEMPO confined ionic liquid : an efficient catalyst system for transition-metal-free aerobic oxidation of alcohols with improved, Org. Biomol. Chem. 9 (2011) 4194–4198.
[43] C.M. Brown, D.J. Lundberg, J.R. Lamb, I. Kevlishvili, D. Kleinschmidt, Y.S. Alfaraj, H.J. Kulik, M.F. Ottaviani, N.J. Oldenhuis, J.A. Johnson, Endohedrally functionalized metal-organic cage-cross-linked polymer gels as modular heterogeneous catalysts, J. Am. Chem. Soc. 144 (2022) 13276–13284.
[44] M. Wang, Z. Xu, Y. Shi, F. Cai, J. Qiu, G. Yang, Z. Hua, T. Chen, TEMPO-functionalized nanoreactors from bottlebrush copolymers for the selective oxidation of alcohols in water, J. Organomet. Chem. 86 (2021) 8027–8035.
[45] Z. Hu, F.M. Kerton, Room temperature aerobic oxidation of alcohols using CuBr 2 with TEMPO and a tetradentate polymer based pyridyl-imine ligand, Appl. Catal. A Gen. 413–414 (2012) 332–339.
[46] D. Tsuchiya, M. Tabata, K. Moriyama, Efficient Swern oxidation and Corey e Kim oxidation with ion-supported methyl sulfoxides and methyl sulfides, Tetrahedron 68 (2012) 6849–6855.
[47] K. Moriyama, M. Takemura, H. Togo, Selective oxidation of alcohols with alkali metal bromides as bromide catalysts: experimental study of the reaction mechanism, J. Organomet. Chem. 79 (2014) 6094–6104.